Electronic Supplementary Material (ESI) for Dalton Transactions.


# Ionic liquids directed syntheses of water-stable Eu- and Tb-organic-frameworks for aqueous-phase detection of nitroaromatic explosives

**Jian-Hua Qin,[a,b] Bing Ma,[a] Xiao-Fei Liu,[a] Hong-Lin Lu,[a] Xi-Yan Dong,[a] Shuang-Quan Zang*[a] and Hongwei Hou*[a]**

[a] *College of Chemistry and Molecular Engineering, Zhengzhou University, Zhengzhou 450001, China.*

[b] *College of Chemistry and Chemical Engineering, Luoyang Normal University, Luoyang 471022, China.*

Author for correspondence:

Prof. S.-Q. Zang, E-mail: zangsqzg@zzu.edu.cn;

Prof. H.-W. Hou, E-mail: houhongw@zzu.edu.cn.

# Supporting Information

**Fig. S1** Supporting structure figure.

**Fig. S2** Thermogravimetric curves of **1** and **2**.

**Fig. S3-S4** Excited state calculation.

**Fig. S5** Solid-state excitation and emission spectra for $H_3BTB$.

**Fig. S6-S7** The fluorescence decay curves for **1** and **2**.

**Fig. S8-S20** Details of detecting of nitroaromatic explosives in the aqueous phase.

**Fig. S21-S22** The band like diffuse reflectance spectra of solid samples of **1** and **2**.

**Fig. S23** The absorption spectrum of the selected analytes in water.

**Table S1.** Crystallographic data and structure refinement details for **1** and **2**.

**Table S2**. Selected bond lengths (Å) and angles (°) for **1** and **2**.

**Table S3**. Saturated vapor pressure for each of the analytes at room temperature (25 ℃).

**Table S4**. Approximate sizes of selected analytes.

**Table S5**. HOMO and LUMO energies calculated for $H_3BTB$ and nitroaromatic explosives at B3LYP/6-31G** level of theory.

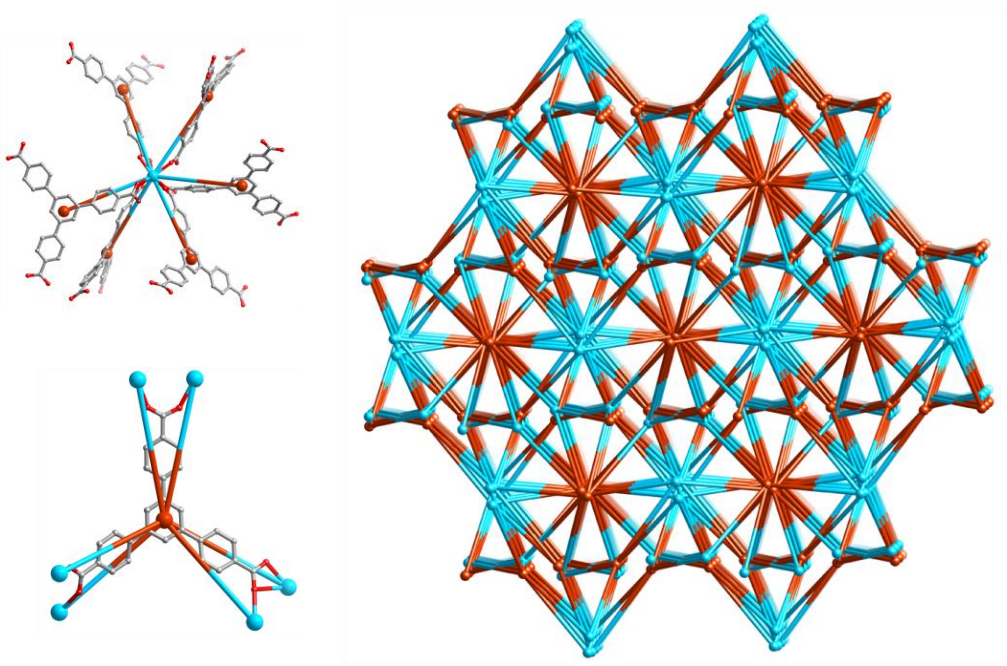

**Fig. S1** Schematic representation of the 6-connected $(4^4.6^7.8^4)(4^8.6^7)$ topology (orange nodes for BTB ligands and cyan nodes for Eu(III) centers).

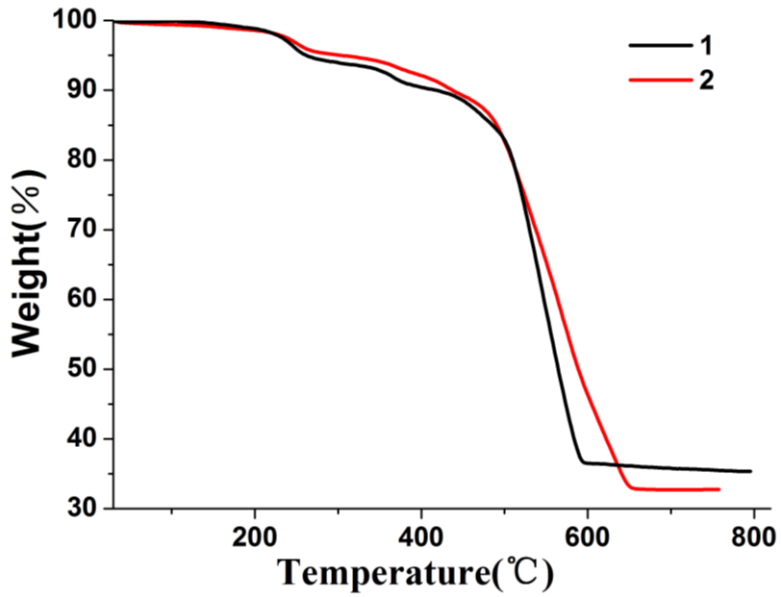


**Fig. S2** Thermogravimetric curves of **1** and **2**.

**Excited state calculation**

The molecular geometry of free ligand $H_3BTB$ was optimized using density functional theory (DFT) at the B3LYP/6-31G* level, as shown in Fig. S3. Based on the optimized geometry, the energy of the lowest triplet excited state of $H_3BTB$ was calculated to be 2.9044 eV (23426 $cm^{-1}$) using the time-dependent DFT approach. All the calculations were performed in Gaussian03 software. Using the same approach, the molecular geometry of ligand BTB coordinating with $Ln^{3+}$ ions was also analyzed (Fig. S4), and the energy of the lowest triplet excited state of BTB was calculated to be 2.9551 eV (23835 $cm^{-1}$).

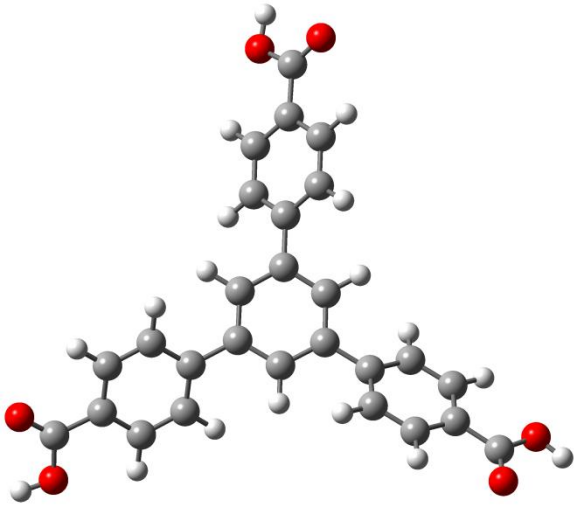

**Fig. S3** The optimized geometry of free ligand $H_3BTB$ at the B3LYP/6-31G* level.

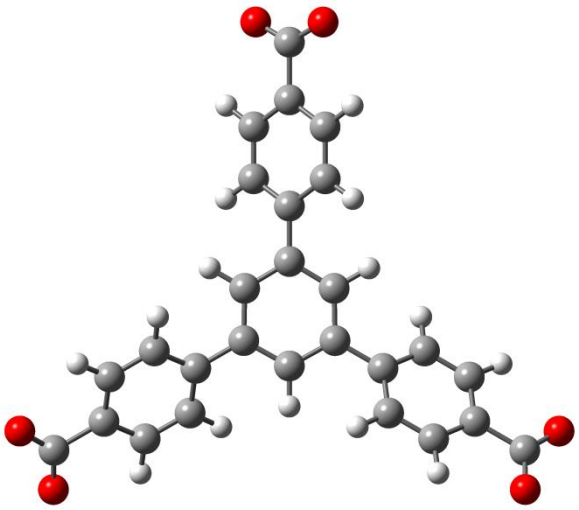

**Fig. S4** The optimized geometry of ligand BTB in MOFs at the B3LYP/6-31G* level.

**Fluorescent properties**

The excitation spectra of **1** and **2** are monitored around the more intense $Ln^{3+}$ emission lines, 610 nm for Eu(III) and 541 nm for Tb(III). It can be seen clearly that the excitation spectrum of **1** consists of a broadband and a weak line. The broadband below 350 nm is due to the charge-transfer between the $O^{2-}$ and Eu(III) ions and $\pi \rightarrow \pi^*$ electron transition of the organic bridging ligands. The excitation spectrum of **2** displays a large broadband with a structured profile in the UV spectral region which is ascribed to the electronic transitions of organic ligands. The absolute high intensity of the broadband compared to that of the intra4f$^n$ lines indicates that the $\pi \rightarrow \pi^*$ electron transition of the organic bridging ligands is a dominant path to sensitizing Eu(III)/Tb(III) excited states.

Complexes **1** and **2** emit red and green fluorescence, respectively. As is well known, the $^5D_0 \rightarrow {}^7F_2$ transition of Eu(III) is hypersensitive to site symmetry and of the electric-dipole (ED) nature, while the $^5D_0 \rightarrow {}^7F_1$ transition is insensitive to site symmetry and the magnetic-dipole (MD) nature according to Judd-Ofelt theory. Besides, the $^5D_0 \rightarrow {}^7F_0$ transition of Eu(III) is invisible in the emission spectrum, which is only allowed for Cs, Cn, and Cnv site symmetries according to the ED selection rule. These experimental facts thus suggest that the Eu(III) ion in **1** is located at a high-symmetry site, which is in good agreement with our single-crystal X-ray analysis. For **2**, the dominant band of these emissions is attributed to the hypersensitive transition $^5D_4 \rightarrow {}^7F_5$ of Tb(III) ions, while the stronger luminescent band corresponds to $^5D_4 \rightarrow {}^7F_6$ transition, and the two less intense bands are ascribed to $^5D_4 \rightarrow {}^7F_4$ and $^5D_4 \rightarrow {}^7F_3$ transitions, respectively. The $^5D_4 \rightarrow {}^7F_J$ ($J$ = 2−0) transitions are measured with weak intensity. It is worth noting that there is no apparent residual ligand-based emission in the 400−450 nm region, indicating the energy transfer from the ligand to the lanthanide center is very effective and can sensitize the lanthanide emission to a large extent.

The emission quantum yields were measured at room temperature under the excitation wavelengths that maximize the emissions of lanthanide cations. As a result, the quantum yields are 19.2% for **1** and 0.6% for **2**. The fluorescence decay curves of **1** and **2** were also obtained at room temperature (Fig. S6 and S7). The corresponding lifetime for **1** is about $\tau1$ = 0.53 (100%) ms, and that for **2** is about $\tau1$ = 0.22 (86.86%) ms and $\tau2$ = 0.98 (13.14%) ms (determined by monitoring $^5D_0 \rightarrow {}^7F_2$ line for **1** and $^5D_4 \rightarrow {}^7F_5$ line for **2** excited at 350nm). Complexes **1** and **2** both have a relatively long quantum yield and a fluorescence lifetime. Because the excitations now fall in the range of those commercially available, they could be good candidates for light-emitting diodes (LEDs) and light applications.

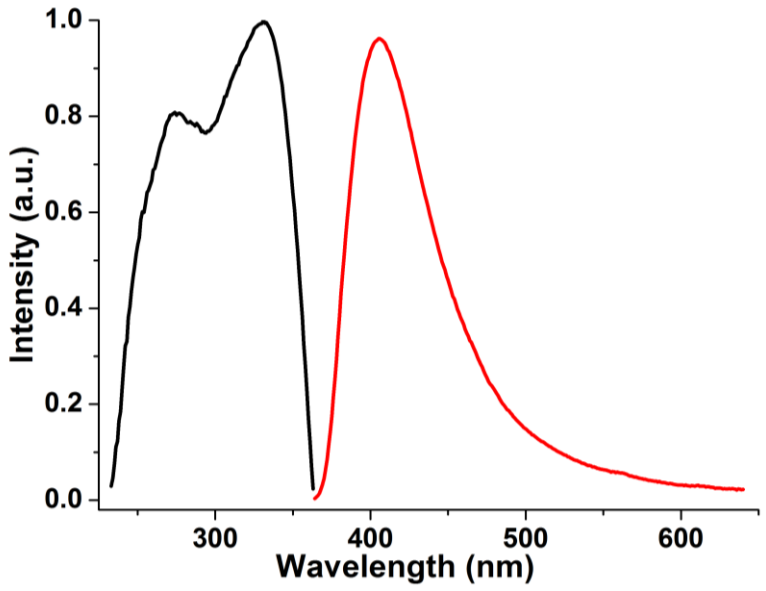


**Fig. S5** Solid-state emission spectra for $H_3BTB$ at room temperature.

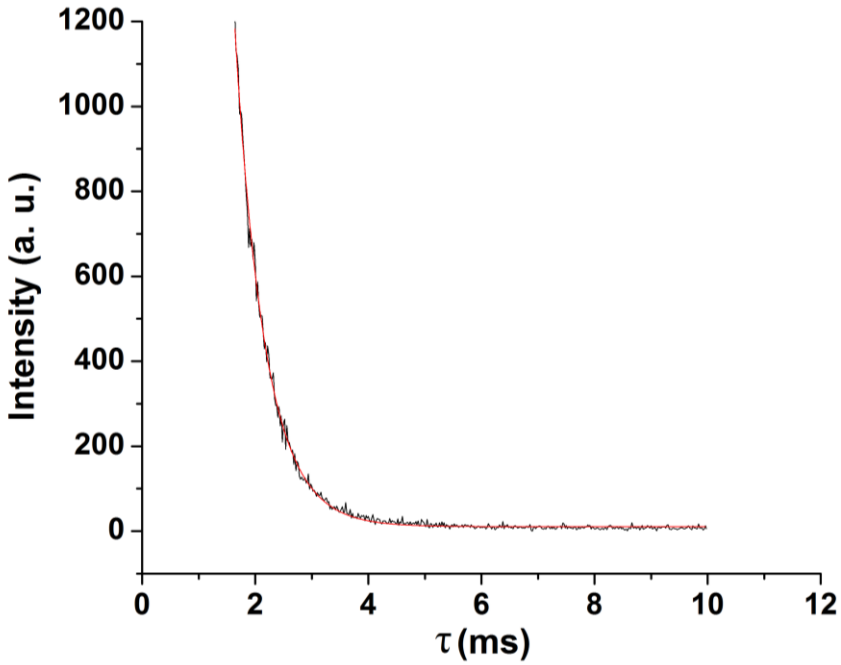


**Fig. S6** The fluorescence decay curve for **1**.

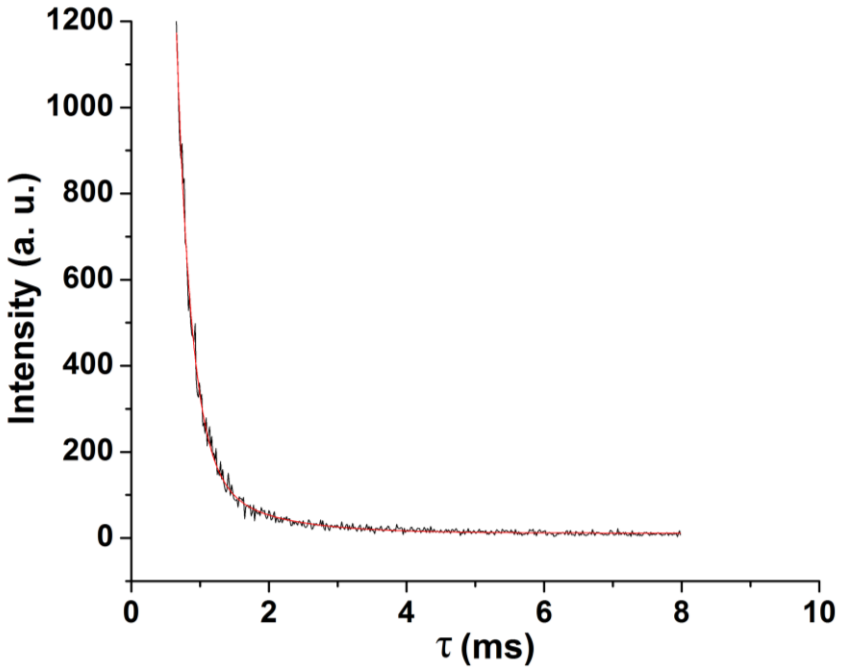


**Fig. S7** The fluorescence decay curve for **2**.

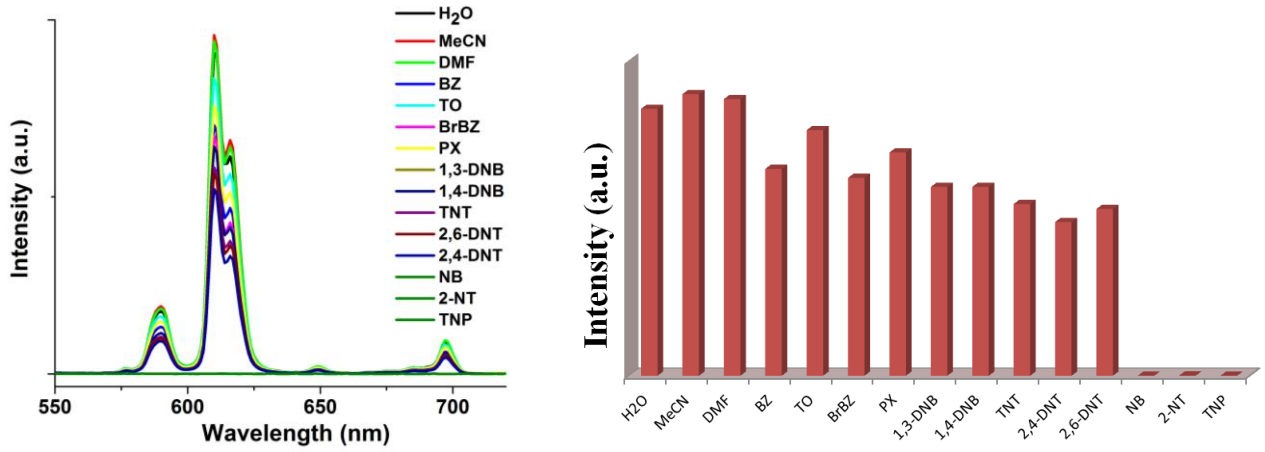


(a) (b)

**Fig. S8** The emission spectra (a) and the fluorescent intensity (b) for **1** dispersed in $H_2O$, MeCN, DMF, BZ, TO, BrBZ, PX, and 1 mM or saturated aqueous solutions of eight different analytes at room temperature.

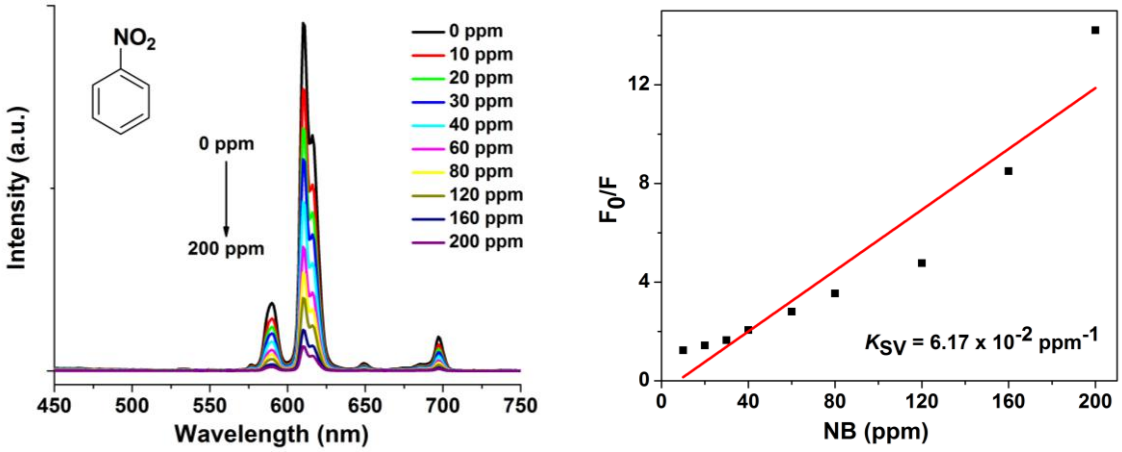


(a) (b)

**Fig. S9** (a) Fluorescence titration of **1** dispersed in aqueous solution by gradual addition of NB.

(b) Stern-Volmer plot of $F_0/F$ *vs.* NB concentration in aqueous solution for **1**.

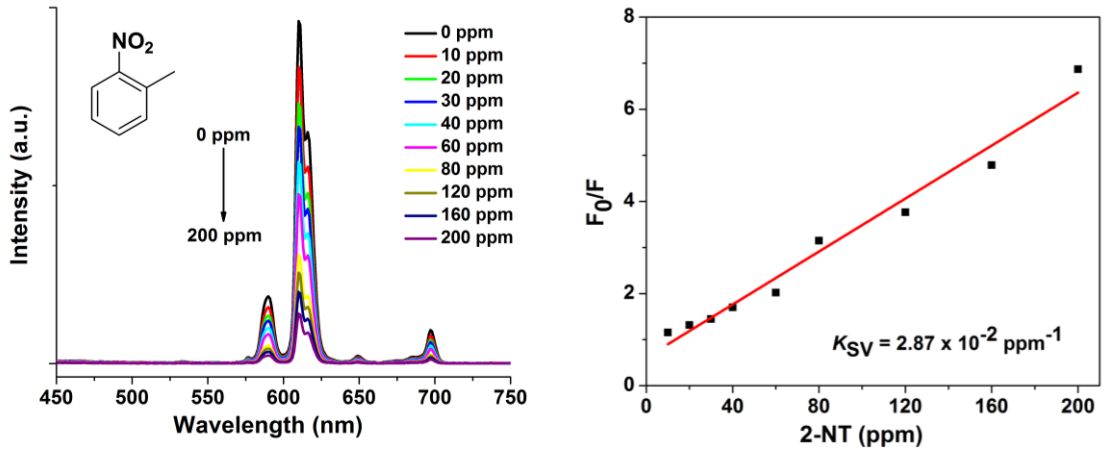


(a) (b)

**Fig. S10** (a) Fluorescence titration of **1** dispersed in aqueous solution by gradual addition of 2-NT.

(b) Stern-Volmer plot of $F_0/F$ *vs.* 2-NT concentration in aqueous solution for **1**.

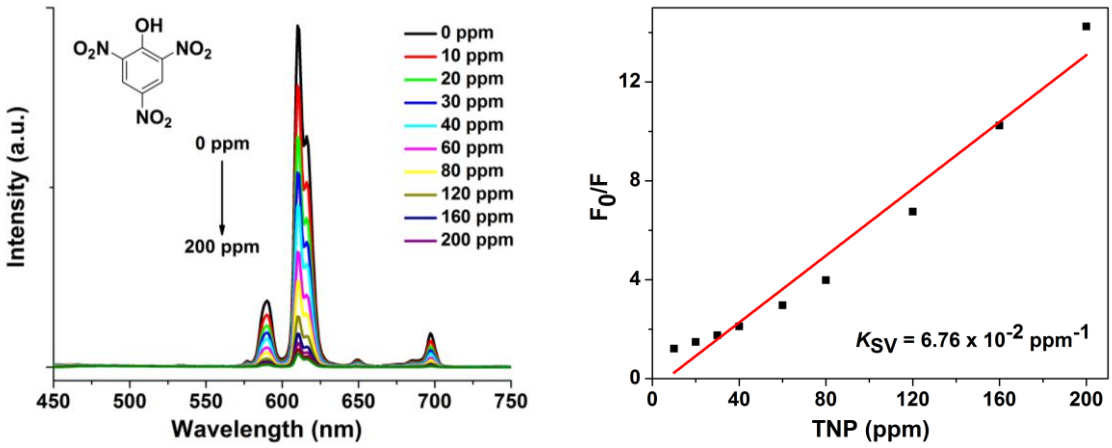


(a) (b)

**Fig. S11** (a) Fluorescence titration of **1** dispersed in aqueous solution by gradual addition of TNP.

(b) Stern-Volmer plot of $F_0/F$ *vs.* TNP concentration in aqueous solution for **1**.

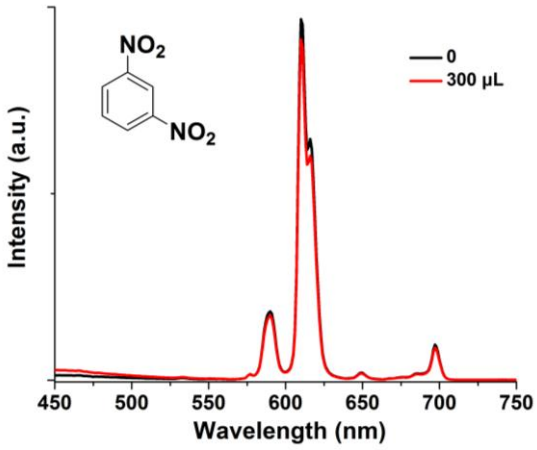


(a)

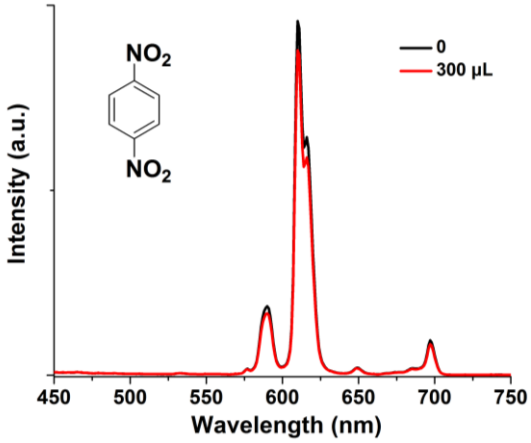


(b)

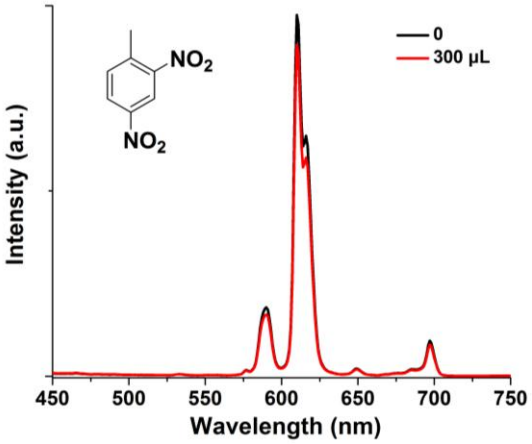


(c)

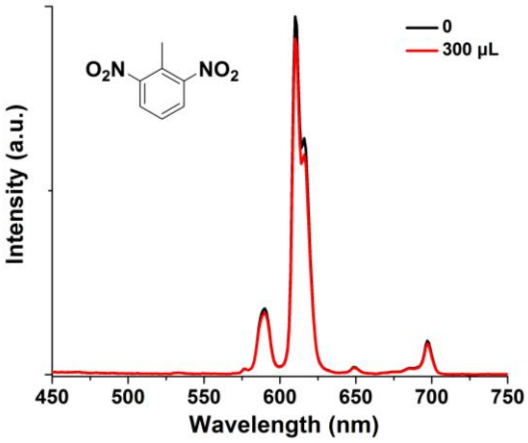


(d)

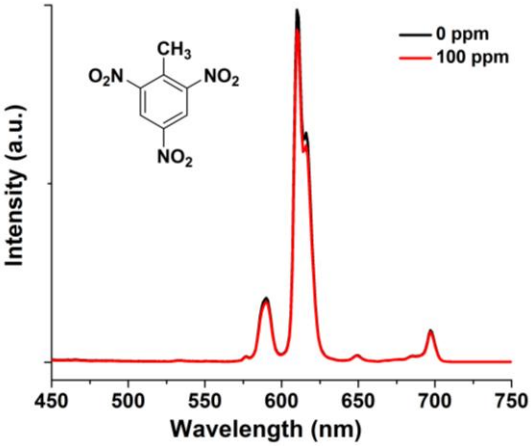


(e)

**Fig. S12** Fluorescence titration of **1** dispersed in aqueous solution by gradual addition of saturated aqueous solutions of 1,3-DNB (a), 1,4-DNB (b), 2,4-DNT (c), 2,6-DNT (d), and TNT(e)

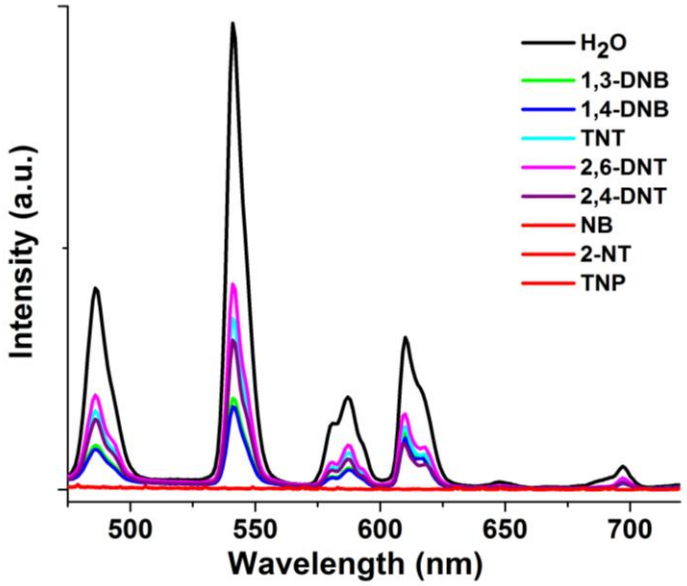


**Fig. S13** The emission spectra for **2** dispersed in $H_2O$ and 1 mM or saturated aqueous solutions of the selected analytes at room temperature.

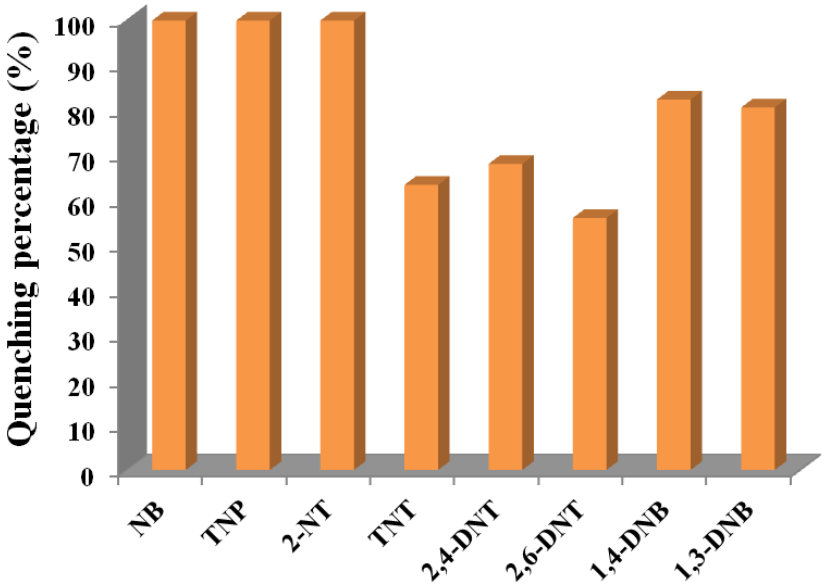


**Fig. S14** Quenching efficiency of the fluorescent intensity for **2** dispersed in 1 mM or saturated aqueous solutions of the selected analytes at room temperature. (excited and monitored at 300 nm and 541 nm, respectively).

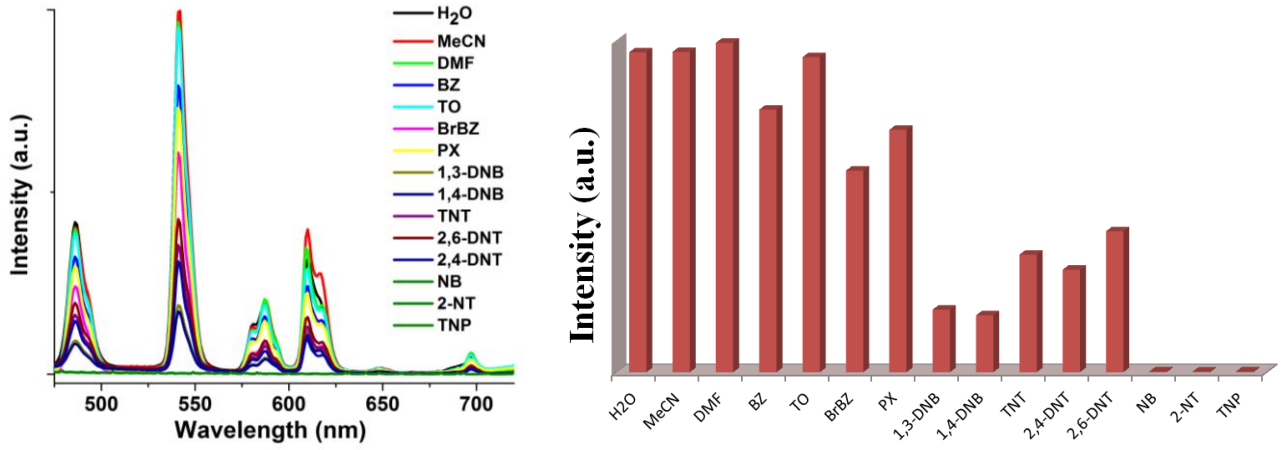


(a) (b)

**Fig. S15** The emission spectra (a) and the fluorescent intensity (b) for **2** dispersed in $H_2O$, MeCN, DMF, BZ, TO, BrBZ, PX, and 1 mM or saturated aqueous solutions of eight different analytes at room temperature.

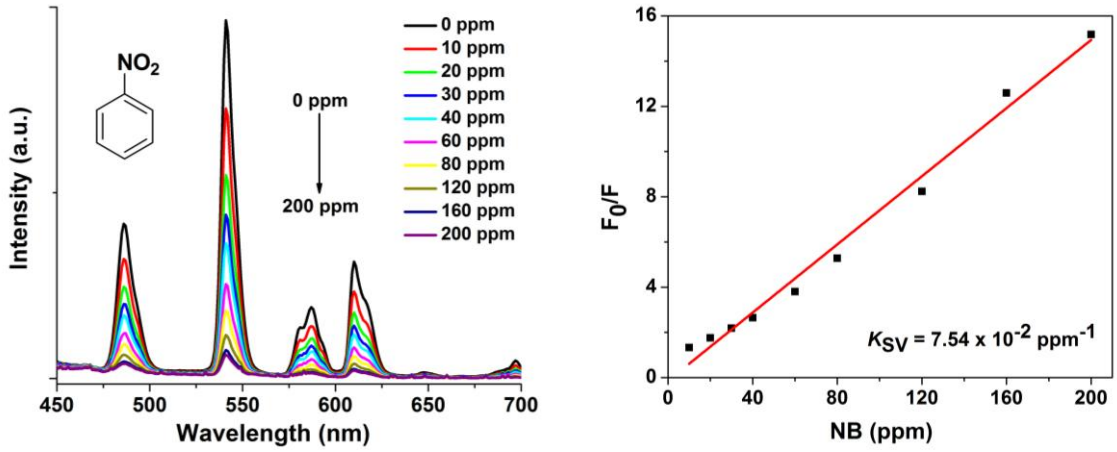


(a) (b)

**Fig. S16** (a) Fluorescence titration of **2** dispersed in aqueous solution by gradual addition of NB.

(b) Stern-Volmer plot of $F_0/F$ *vs.* NB concentration in aqueous solution for **2**.

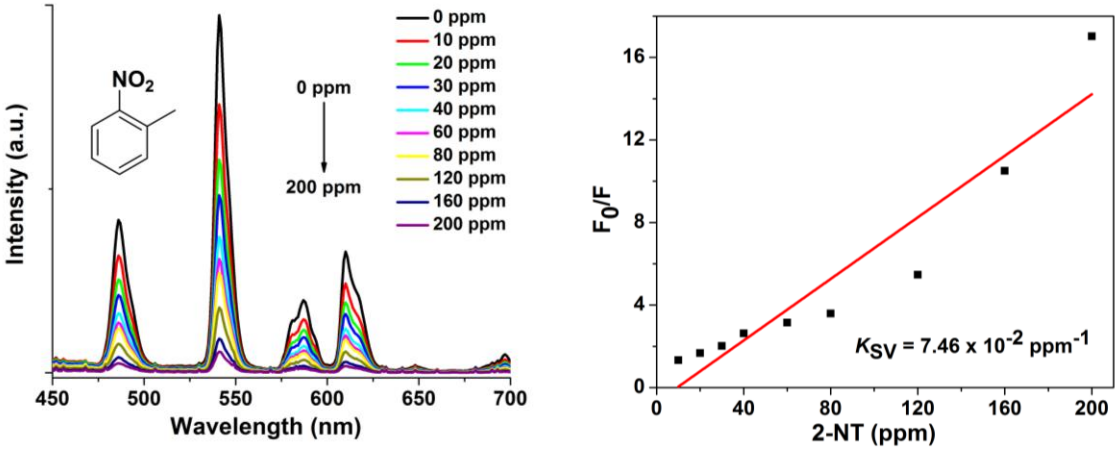


(a) (b)

**Fig. S17** (a) Fluorescence titration of **2** dispersed in aqueous solution by gradual addition of 2-NT.

(b) Stern-Volmer plot of $F_0/F$ *vs.* 2-NT concentration in aqueous solution for **2**.

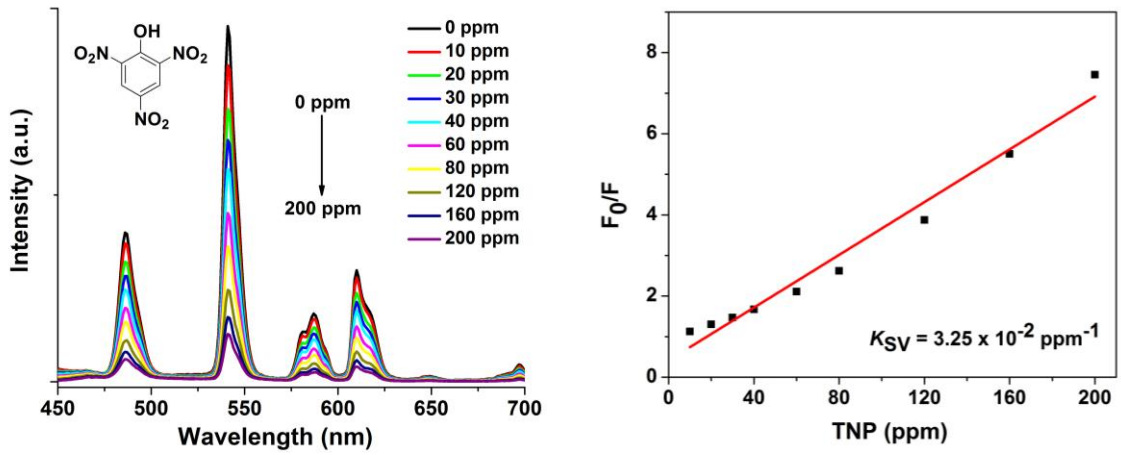


(a) (b)

**Fig. S18** (a) Fluorescence titration of **2** dispersed in aqueous solution by gradual addition of TNP.

(b) Stern-Volmer plot of $F_0/F$ *vs.* TNP concentration in aqueous solution for **2**.

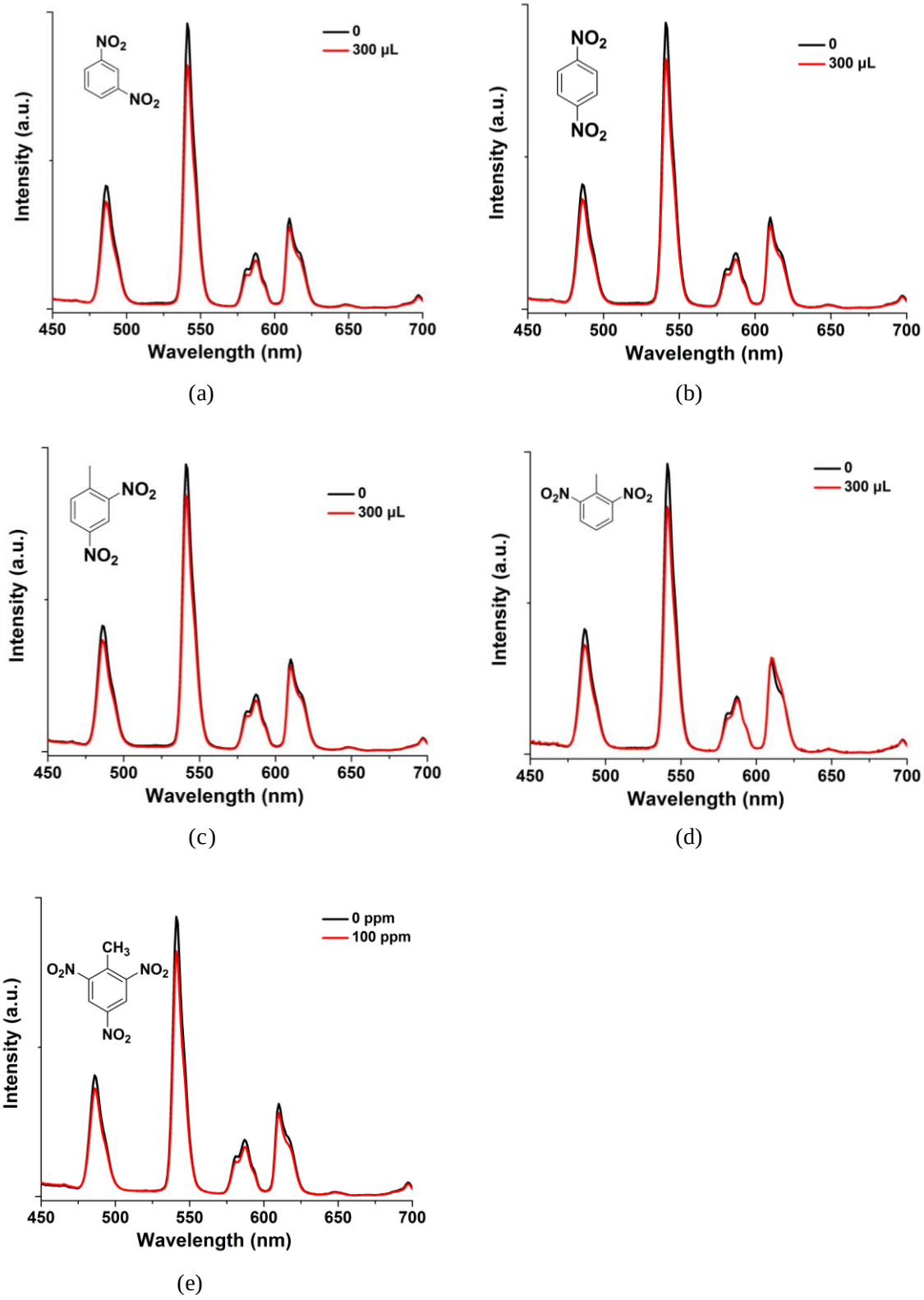


**Fig. S19** Fluorescence titration of **2** dispersed in aqueous solution by gradual addition of saturated aqueous solutions of 1,3-DNB (a), 1,4-DNB (b), 2,4-DNT (c), 2,6-DNT (d), and TNT(e)

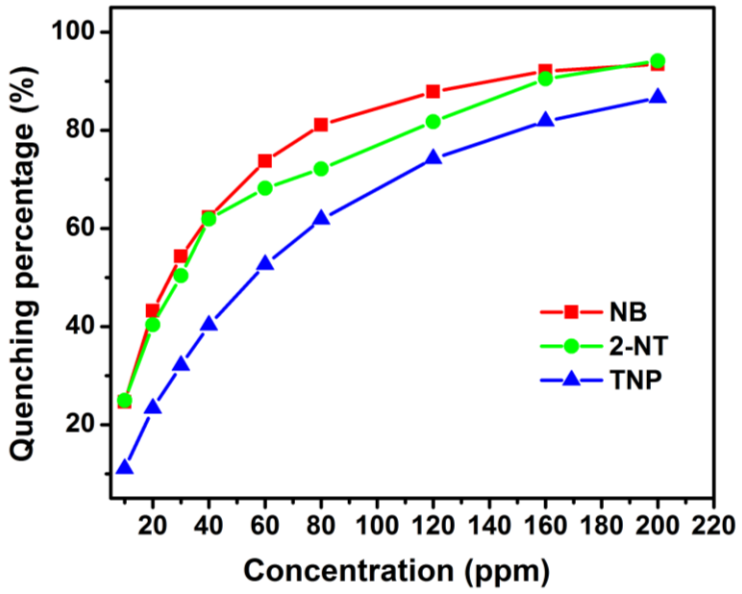


**Fig. S20** Quenching efficiency of **2** dispersed in aqueous solutions at different concentrations of NB, 2-NT, and TNP.

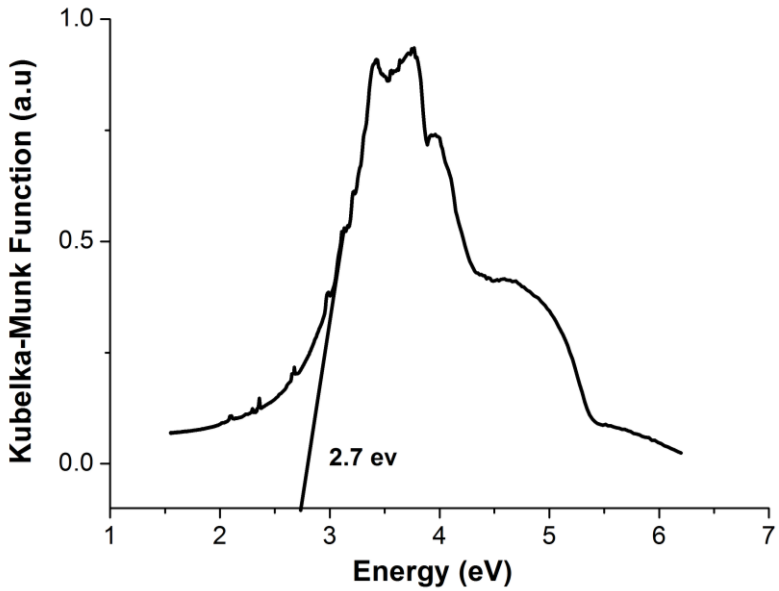


**Fig. S21** The band like diffuse reflectance spectrum of a solid sample of **1**.

The optical band gap is estimated to be ~2.7 eV.

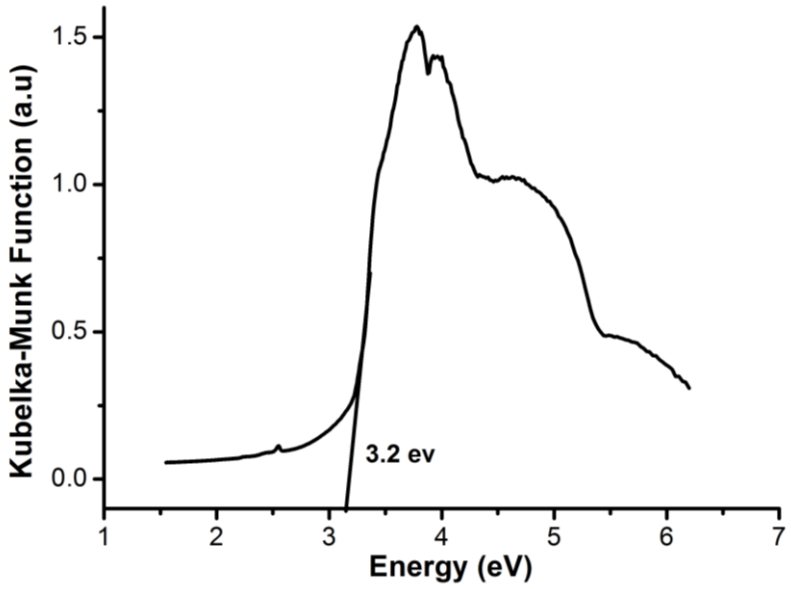


**Fig. S22** The band like diffuse reflectance spectrum of a solid sample of **2**.

The optical band gap is estimated to be ~3.2 eV.

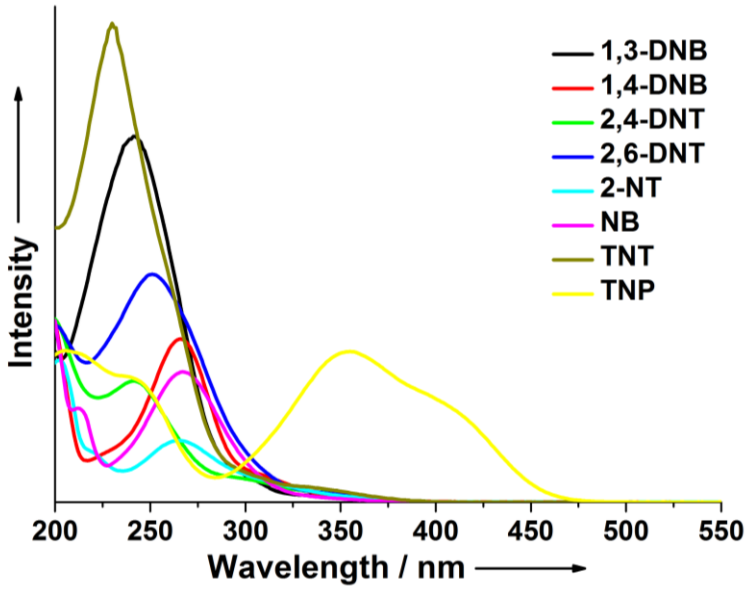


**Fig. S23** The absorption spectrum of the selected analytes in water.

**Table S1.** Crystallographic data and experimental details for **1** and **2**.

| Complex | **1** | **2** |
|---|---|---|
| Formula | $C_{27}H_{17}EuO_7$ | $C_{27}H_{17}TbO_7$ |
| Formula weight | 605.37 | 612.33 |
| Crystal system | Orthorhombic | Orthorhombic |
| Space group | *Fddd* | *Fddd* |
| a (Å) | 22.543(5) | 22.482(5) |
| b (Å) | 29.134(6) | 28.996(6) |
| c (Å) | 29.168(6) | 29.067(6) |
| V (Å$^3$) | 19157(7) | 18949(7) |
| Z | 32 | 32 |
| $D_c$ (g/cm$^3$) | 1.679 | 1.717 |
| Abs coeff/mm$^{-1}$ | 2.664 | 3.031 |
| F(000) | 9536 | 9600 |
| θ range for data collection (°) | 2.68/25.50 | 2.69/25.50 |
| Data/restraints/parameters | 4365/53/316 | 4326/84/316 |
| GOF | 1.253 | 1.085 |
| $R$ [$I > 2\sigma(I)$] | $R_1$ = 0.0727<br>$wR_2$ = 0.1546 | $R_1$ = 0.0789<br>$wR_2$ = 0.2922 |
| $R$ (all data) | $R_1$ = 0.0755<br>$wR_2$ = 0.1564 | $R_1$ = 0.0860<br>$wR_2$ = 0.3034 |

$R = [\sum ||F_0| - |F_d|| / \sum |F_0|]$, $R_W = \sum_W [|F_0^2 - Fc^2|^2 / \sum_W (|F_w|^2)^2]^{1/2}$

**Table S2**. Selected bond lengths (Å) and angles (°) for **1** and **2**

| Complex **1** | | | |
|---|---|---|---|
| Eu(1)-O(4)#1 | 2.300(7) | Eu(1)-O(2)#5 | 2.391(6) |
| Eu(1)-O(5)#2 | 2.331(8) | Eu(1)-O(1) | 2.397(6) |
| Eu(1)-O(6)#3 | 2.333(7) | Eu(1)-O(7) | 2.505(6) |
| Eu(1)-O(3)#4 | 2.338(7) | Eu(1)-O(2) | 2.809(8) |
| O(4)#1-Eu(1)-O(5)#2 | 120.5(3) | O(2)#5-Eu(1)-O(1) | 125.6(3) |
| O(4)#1-Eu(1)-O(6)#3 | 87.0(3) | O(4)#1-Eu(1)-O(7) | 76.4(3) |
| O(5)#2-Eu(1)-O(6)#3 | 132.7(3) | O(5)#2-Eu(1)-O(7) | 143.7(4) |
| O(4)#1-Eu(1)-O(3)#4 | 82.4(3) | O(6)#3-Eu(1)-O(7) | 75.5(4) |
| O(5)#2-Eu(1)-O(3)#4 | 76.6(3) | O(3)#4-Eu(1)-O(7) | 74.2(4) |
| O(6)#3-Eu(1)-O(3)#4 | 149.4(3) | O(2)#5-Eu(1)-O(7) | 144.2(4) |
| O(4)#1-Eu(1)-O(2)#5 | 79.0(3) | O(1)-Eu(1)-O(7) | 75.8(3) |
| O(5)#2-Eu(1)-O(2)#5 | 71.9(3) | O(4)#1-Eu(1)-O(2) | 147.0(2) |
| O(6)#3-Eu(1)-O(2)#5 | 77.6(3) | O(5)#2-Eu(1)-O(2) | 72.0(3) |
| O(3)#4-Eu(1)-O(2)#5 | 127.6(3) | O(6)#3-Eu(1)-O(2) | 66.3(3) |
| O(4)#1-Eu(1)-O(1) | 152.3(3) | O(3)#4-Eu(1)-O(2) | 130.3(2) |
| O(5)#2-Eu(1)-O(1) | 82.9(3) | O(2)#5-Eu(1)-O(2) | 76.8(2) |
| O(6)#3-Eu(1)-O(1) | 86.5(3) | O(1)-Eu(1)-O(2) | 49.4(2) |
| O(3)#4-Eu(1)-O(1) | 89.7(3) | O(7)-Eu(1)-O(2) | 112.4(3) |
| Complex **2** | | | |
| Tb(1)-O(4)#1 | 2.267(7) | Tb(1)-O(1) | 2.346(7) |
| Tb(1)-O(6)#2 | 2.292(8) | Tb(1)-O(2)#5 | 2.355(6) |
| Tb(1)-O(5)#3 | 2.309(7) | Tb(1)-O(7) | 2.455(7) |
| Tb(1)-O(3)#4 | 2.320(8) | Tb(1)-O(2) | 2.822(7) |
| O(4)#1-Tb(1)-O(6)#2 | 86.0(3) | O(1)-Tb(1)-O(2)#5 | 125.1(3) |
| O(4)#1-Tb(1)-O(5)#3 | 119.3(3) | O(4)#1-Tb(1)-O(7) | 76.4(3) |
| O(6)#2-Tb(1)-O(5)#3 | 133.5(3) | O(6)#2-Tb(1)-O(7) | 74.8(3) |
| O(4)#1-Tb(1)-O(3)#4 | 83.3(3) | O(5)#3-Tb(1)-O(7) | 144.8(3) |
| O(6)#2-Tb(1)-O(3)#4 | 149.4(3) | O(3)#4-Tb(1)-O(7) | 74.8(3) |
| O(5)#3-Tb(1)-O(3)#4 | 76.2(3) | O(1)-Tb(1)-O(7) | 77.6(3) |

| | | | |
|---|---|---|---|
| O(4)#1-Tb(1)-O(1) | 154.1(3) | O(2)#5-Tb(1)-O(7) | 143.6(3) |
| O(6)#2-Tb(1)-O(1) | 87.9(3) | O(4)#1-Tb(1)-O(2) | 146.3(2) |
| O(5)#3-Tb(1)-O(1) | 82.5(3) | O(6)#2-Tb(1)-O(2) | 67.2(3) |
| O(3)#4-Tb(1)-O(1) | 89.3(3) | O(5)#3-Tb(1)-O(2) | 72.2(2) |
| O(4)#1-Tb(1)-O(2)#5 | 78.1(3) | O(3)#4-Tb(1)-O(2) | 130.1(2) |
| O(6)#2-Tb(1)-O(2)#5 | 77.9(3) | O(1)-Tb(1)-O(2) | 49.4(2) |
| O(5)#3-Tb(1)-O(2)#5 | 71.2(3) | O(2)#5-Tb(1)-O(2) | 76.5(2) |
| O(3)#4-Tb(1)-O(2)#5 | 127.2(3) | O(7)-Tb(1)-O(2) | 113.4(2) |

Symmetry transformations used to generate equivalent atoms for complex **1**: #1 -x+7/4, y+1/2, -z+5/4; #2 -x+9/4, -y+7/4, z-1/2; #3 x-1/4, y+1/4, -z+3/2; #4 x+1/2, -y+7/4, -z+5/4 ; #5 -x+2, -y+2, -z+1. For complex **2**: #1 -x+7/4, y+1/2, -z+5/4; #2 x-1/4, y+1/4, -z+3/2; #3 x+1/2, -y+7/4, -z+5/4; #4 -x+9/4, -y+7/4, z-1/2; #5 -x+2, -y+2, -z+1.

**Table S3**. Saturated vapor pressure for each of the analytes at room temperature (25 ℃).

| **Analytes** | **Vapor Pressure (in mmHg)** | **Reduction Potential (in V *vs* SCE)** |
|---|---|---|
| Nitrobenzene (NB)[1] | 0.2416 | −1.15 |
| 2-Nitrotoluene (2-NT)[1] | 0.1602 | −1.2 |
| 1,3-Dinitrobenzene(1,3-DNB)[2] | $8.82 \times 10^{-4}$ | −0.9 |
| 1,4-Dinitrobenzene (1,4-DNB)[1] | $2.406 \times 10^{-5}$ | −0.7 |
| 2,4-dinitrotoluene (2,4-DNT)[1] | $1.44 \times 10^{-4}$ | −1.0 |
| 2,6-dinitrotoluene (2,6-DNT)[1,3] | $5.61 \times 10^{-4}$ | −1.0 |
| 2,4,6-trinitrotoluene (TNT)[1,4] | $8.02 \times 10^{-6}$ | −0.7 |
| 2,4,6-trinitrophenol (TNP)[4] | $5.8 \times 10^{-9}$ | −0.63 |


1 J. S. Yang and T. M. Swager, *J. Am. Chem. Soc.*, 1998, **120**, 11864.

2 R. Hoffmann, *J. Chem. Phys.*, 1963, **39**, 1397.

3 A. J. Lan, K. H. Li, H. H. Wu, L. Z. Kong, N. Nijem, D. H. Olson, T. J. Emge, Y. J. Chabal, D. C. Langreth, M. C. Hong and J. Li, *Inorg. Chem.*, 2009, **48**, 7165.

4 J. C. Sanchez and W. C. Trogler, *J. Mater. Chem.*, 2008, **18**, 3143.

**Table S4**. Approximate sizes of the selected analytes.

| Analytes | Approximate Size (D ×W×L, Å) |
|---|---|
| NB | 3.4 × 6.2 × 8.6 |
| 2-NT | 5.0 × 7.7 × 8.6 |
| 1,3-DNB | 5.6 × 7.7 × 8.1 |
| 1,4-DNB | 5.6 × 7.7 × 9.1 |
| 2,4-DNT | 5.6 × 7.7 × 10.1 |
| 2,6-DNT | 5.6 × 7.7 × 9.5 |
| TNT | 5.6 × 7.7 × 10.2 |
| TNP | 5.0 × 6.2 × 7.1 |

**Table S5**. HOMO and LUMO energies calculated for $H_3BTB$ and nitroaromatic explosives at B3LYP/6-31G** level of theory.

| Analytes | HOMO (eV) | LUMO (eV) | Band gap |
|---|---|---|---|
| $H_3BTB$ | -6.73074 | -2.00385 | 4.72689 |
| NB[6] | -7.5912 | -2.4283 | 5.1629 |
| 2-NT[5] | -7.36454 | -2.31722 | 5.04732 |
| 1,3-DNB[6] | -7.9855 | -3.4311 | 4.5544 |
| 1,4-DNB[5] | -8.35250 | -3.49679 | 4.85571 |
| 2,4-DNT[6] | -7.7645 | -3.2174 | 4.5471 |
| 2,6-DNT[6] | -7.6448 | -3.2877 | 4.3571 |
| TNT[6] | -8.2374 | -3.8978 | 4.3396 |
| TNP[6] | -8.4592 | -3.4926 | 4.9666 |

5 G. Y. Wang, C. Song, D. M. Kong, W. J. Ruan, Z. Chang and Y. Li, *J. Mater. Chem. A.*, 2014, **2**, 2213.

6 S. S. Nagarkar, B. Joarder, A. K. Chaudhari, S. Mukherjee and S. K. Ghosh, *Angew. Chem., Int. Ed.*, 2013, **52**, 2881.